Radiation Measurements 68 (2014) 23–30

Contents lists available at ScienceDirect

Radiation Measurements

journal homepage: www.elsevier.com/locate/radmeas

Visualization of high radiation field by radiophotoluminescence photography

Fuminobu Sato [a, *], Naoki Zushi [a], Tatsuro Maekawa [a], Yushi Kato [a], Isao Murata [a], Kikuo Shimizu [b], Takayoshi Yamamoto [c], Toshiyuki Iida [a]

[a] Graduate School of Engineering, Osaka University, 2-1 Yamadaoka, Suita, Osaka 565-0871, Japan
[b] Radioisotope Research Center, Osaka University, 1-1 Machikaneyama, Toyonaka, Osaka 560-0043, Japan
[c] Oarai Research Center, Chiyoda Technol Corporation, 3681 Narita, Oarai, Higashiibaraki, Ibaraki 311-1313, Japan

HIGHLIGHTS

- A formation model of radiophotoluminescence (RPL) centers has been proposed.
- The activation energies of the formation of RPL centers were determined.
- We developed a simple and radiation-proof RPL photographing technique.
- The RPL photography is useful for the visualization of high radiation fields.

ARTICLE INFO

Article history:
Received 23 March 2014
Received in revised form
20 June 2014
Accepted 21 June 2014
Available online 15 July 2014

Keywords:
Radiophotoluminescenc dosimeter
Radiophotoluminescence property
Radiophotoluminescence photography
Visualization of high radiation field
The Fukushima Daiichi nuclear plant accident

ABSTRACT

We have proposed a simple technique for the visualization of high radiation fields by radiophotoluminescence (RPL) photography. Pulverized RPL glass particles were encapsulated into hundreds of polystyrene balls of accumulation-type RPL detectors. The RPL detectors were placed near an intense gamma-ray source. After irradiation, the RPL detectors were uniformly brightened with a UV illuminator. Orange RPL could be observed by the naked eye at doses above 5 Gy. For a dose above 0.5 Gy, a clear RPL photograph was taken with a digital camera. The spatial dose distribution was obtained through digital image processing of the RPL photograph. Therefore, this simple RPL photographing technique using RPL detectors is useful for detecting high levels of radioactivity.

1. Introduction

Large quantities of radioactive particles were released from the Fukushima Daiichi nuclear plant (F1) into the natural environment. High levels of radioactivity prevent workers from approaching the broken nuclear power plant. The spatial distribution of the radioactivity is complex because of the damage caused by gas explosions and the leakage of contaminated water. Workers at the F1 have frequently encountered leaked contaminated water, which is emitting radiation at over 1 Sv/h. Radiation monitoring in the broken nuclear power plant is an important task for the primary decommissioning stage of the F1. Therefore, a simple detection technique for high-level radioactivity is necessary for radiation safety management.

The visualization of high radiation fields contributes substantially to the radiation safety management of the F1. However, fragile visualization systems, such as gamma cameras, cannot be used in high radiation fields. For example, the weight of a typical gamma camera is over 50 kg due to the lead blocks that are used for radiation collimating and shielding. In high-level radiation fields, large numbers of radiation shielding blocks effectively decrease the background noise. In addition, some semiconductor devices installed in the gamma camera are damaged by radiation. When a gamma camera was installed in a remote robot exploring the F1, the weight on board was one of the most significant problems. Consequently, a simple and radiation-proof visualization technique for high radiation fields is desirable for the decommissioning of the F1.

* Corresponding author.
E-mail address: fsato@eei.eng.osaka-u.ac.jp (F. Sato).

http://dx.doi.org/10.1016/j.radmeas.2014.06.011

A radiophotoluminescent (RPL) glass detector made of silver-activated phosphate glass is an accumulation-type detector of ionizing radiation (Piesch et al., 1986). RPL centers produced in bulk by ionizing radiation have high stability, except against thermal annealing. After a preheating process at an appropriate temperature (Ranogajec-Komor et al., 2008), RPL photons of approximately 635 nm in wavelength are emitted upon exposure to UV light. The RPL glass detector has some advantages compared to other detectors, such as optically stimulated luminescence and thermoluminescent detectors. The RPL response exhibits a high sensitivity and linearity over a wide dose range (Ranogajec-Komor et al., 2008). The RPL measurement can be performed repeatedly without fading (Kurobori and Nakamura, 2012).

In this study, we have proposed an RPL photographing technique for the visualization of high-level radiation fields. The practical RPL property of silver-activated phosphate glass was characterized for the establishment of the RPL photographing technique. The RPL buildup effect was investigated using a photoluminescent system with an X-ray generator. RPL glass particles were encapsulated into a polystyrene ball of an accumulation-type RPL detector. Hundreds of RPL detectors were placed in a high-level radiation field. An RPL photograph was successfully taken with the RPL detectors illuminated by UV light. The spatial dose distribution was determined through digital image processing of the RPL photograph. This RPL photographing technique is a very simple technique for detecting high-level radioactivity. For example, radiation workers at the F1 can visually recognize high-level radioactivity and subsequently avoid unexpected exposure to high doses of radiation.

2. Sample and experimental procedures

2.1. Sample preparation

A rod of RPL glass was made from reagent-grade powders using a melting method (Lee et al., 2011). $NaPO_3$ (1000 g), $Al(PO_3)_3$ (1039 g) and AgCl (44 g) were added to a mullite crucible. The mullite crucible was placed in an electrical furnace, and subsequently, its temperature was gradually increased to 1473 K over the course of 10 h. The melting glass was maintained at this temperature for 5 h for homogenization. After homogenization, the melted mixture was slowly cooled to room temperature over the course of 10 h. The atomic composition by weight in the RPL glass was as follows: O (51%), P (32%), Na (11%), Al (6%), Cl (<0.01%) and Ag (0.1%). The cooled glass was cut into pieces with a rotating diamond saw blade. Several pieces of glass plate of 1 mm in thickness were fabricated by a polishing machine. Most of the glass pieces were pulverized by a jet mill, and the pulverized particles were classified using 75 and 150 μm sieves.

2.2. Optical measurement

The RPL glass plates were exposed to ^{60}Co gamma rays with doses of up to 500 Gy. Optical absorption spectra were measured using an optical absorption spectrometer (QE65Pro-ABS, Ocean optics) and a standard UV–visible light source (DH-2000, Ocean optics). Photoluminescence spectra were obtained using a fluorescence spectrometer (QE65Pro-FL, Ocean optics) and a mercury lamp (365 nm). The fluorescence spectrometer was calibrated with a standard UV–visible light source.

Fig. 1 shows a schematic view of the photoluminescence measurement system with an X-ray generator. The system was mainly composed of a fluorescence microscope, microfocus X-ray tube, heating stage and fluorescence spectrometer (Sato et al., 2008). The maximum voltage and current of the X-ray tube were 50 kV and 1 mA, respectively. The X-rays were collimated by a 1-mm-thick tungsten plate through a hole that was 500 μm in diameter. The X-ray beam spot was observed with an RPL glass plate (Aoi et al., 2009), and its diameter was approximately 500 μm. The position of the X-ray beam spot on an RPL sample was individually adjusted by 4-axes position mechanisms for the X-ray tube and the tungsten collimator. The absorbed dose rate was approximately 0.1 Gy/s for the RPL glass. An RPL glass sample was placed on the heating stage with silver paste. A heating controller maintained the temperature of the RPL glass sample. A dichroic mirror (<400 nm), a fluorescence filter (450–900 nm) and an excitation filter (365 nm) were set in the fluorescence microscope. The RPL glass sample was exposed to UV light from a mercury lamp. During and after the X-ray irradiation, the RPL spectra were measured by the fluorescence spectrometer at a time interval of 10 s. In this study, the RPL intensity R is defined as

$$R(D) = \int_{550}^{750} I(D,\lambda)\mathrm{d}\lambda - \int_{550}^{750} I(0,\lambda)\mathrm{d}\lambda \quad (1)$$

where D is the absorbed dose, λ is the wavelength, and I is the photoluminescence intensity measured by the fluorescence spectrometer.

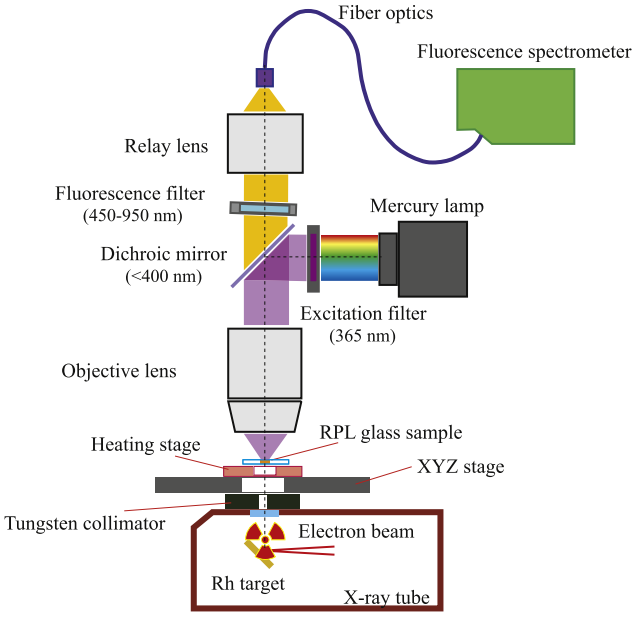

Fig. 1. Photoluminescence measurement system with an X-ray generator. The system is mainly composed of a fluorescence microscope, microfocus X-ray tube, heating stage and fluorescence spectrometer. An RPL glass sample was irradiated using an X-ray beam 500 μm in diameter. During the X-ray irradiation, an objective lens collected photoluminescence from the sample illuminated by 365 nm light from a mercury lamp. The radiophotoluminescence in a wavelength range from 450 to 950 nm was analyzed by a fluorescence spectrometer.

2.3. Radiophotoluminescence photographing technique

The pulverized RPL glass particles were encapsulated into hundreds of polystyrene balls 30 mm in diameter. Polystyrene is radiation-resistant material, and its visible transparency is maintained at high radiation doses. Furthermore, a polypropylene floater 25 mm in diameter was centrically set inside the polystyrene balls, and the thickness of the layer of the RPL glass particles was 1–2 mm. The specific density of the RPL detector was

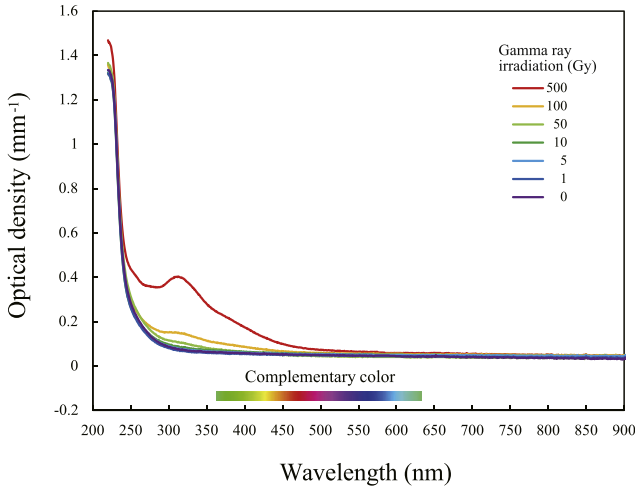

Fig. 2. Optical absorption spectra of RPL glass plates exposed to gamma rays. Optical absorption bands at 315 and 360 nm are observed at high doses. The band at 315 nm is strongly related to RPL excitation. The transparency in the range from 500 to 900 nm was maintained at high doses.

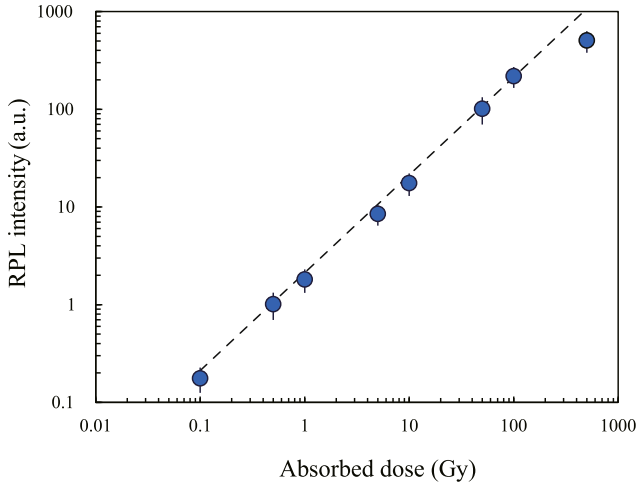

Fig. 4. Relation between absorbed dose and RPL intensity for RPL glass particles. The RPL response had satisfactory linearity up to 100 Gy, although a minimal self-absorption effect for the RPL was observed. The lowest detectable dose was approximately 100 mGy.

slightly lower than that of water because of the use of a polypropylene floater. Therefore, the RPL detector is useful to analyze water contaminated by high-level radioactivity. No optical polishing process is required to make the RPL detector, which is not the case for conventional glass detectors. The RPL detector is easy to manufacture and has good mass production properties. In principle, the RPL detector can only be used once. In contrast, the RPL glass particles can be reused after disassembly of the polystyrene ball.

Hundreds of RPL detectors were placed at 80 mm intervals around a ^{60}Co gamma-ray source of 6 TBq in a 160 × 152 cm area. After irradiation, the RPL detectors were uniformly brightened by a floodlight made of UV light-emitting diodes (LEDs) with a peak wavelength of 365 nm, and photoluminescence images were recorded using a digital camera. The RPL photographing was strongly affected by the conditions of the UV lighting. Specifically, uniform illumination was desirable for determining the dose values with satisfactory accuracy. In addition, fluorescent marker tape was put on each polystyrene ball. During the RPL photography process, blue photons were emitted from the fluorescent marker tape independently of the irradiation dose. Each dose value was roughly corrected by comparing the RPL intensity and the blue fluorescence intensity.

3. Results and discussion

3.1. Radiophotoluminescence property

Fig. 2 shows optical absorption spectra of the RPL glass plates exposed to gamma rays. A preheating process was performed at 343 K for an hour after the gamma-ray irradiation. Optical absorption bands at 315 and 360 nm were observed at high doses. It has been reported that light at 315 nm is most effective for RPL excitation (Miyamoto et al., 2010). In addition, there is no large optical absorption in the wavelength range from 500 to 900 nm.

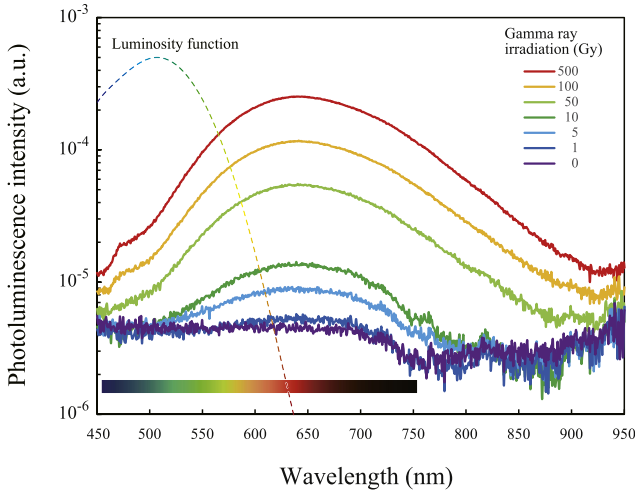

Fig. 3. Photoluminescence spectra of RPL glass particles exposed to gamma rays. A UV illuminator with a peak wavelength of 365 nm was used as an excitation source. The RPL spectra, which were related to the formation of Ag^{++} and Ag^{0} centers, had large, broad peaks at approximately 635 nm. The RPL appeared orange based on the luminosity function with a peak value of unity at 555 nm.

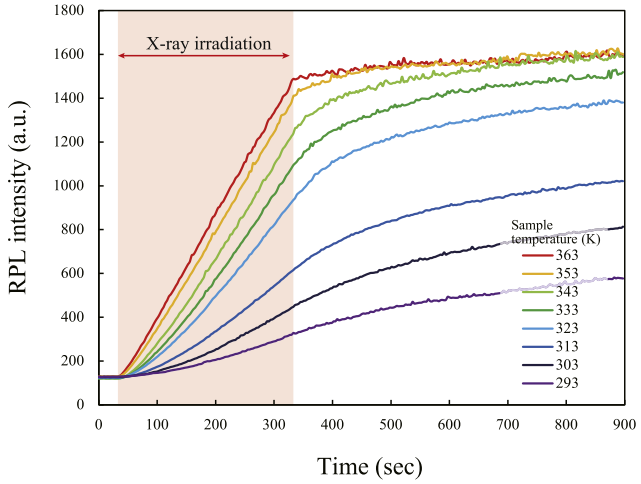

Fig. 5. Changes in RPL intensities at different temperatures. The X-ray generator was operated for 300 s, and the maximum absorbed dose was approximately 5 Gy. The increments of the RPL intensities evidently depended on the sample temperatures. The results suggested that the formation of RPL centers (Ag^{++} and Ag^{0}) had two different temperature dependencies.

Fig. 3 shows the photoluminescence spectra of RPL glass particles exposed to gamma rays. A UV illuminator with a peak wavelength of 365 nm was used as an excitation source. The RPL spectra, which are related to the formation of Ag^{++} and Ag^0 centers (Yokota and Imagawa, 1967), had large, broad peaks at approximately 635 nm. The Ag^0 center is related to electron trapping in the Ag^+ center. Meanwhile, the Ag^{++} center is transferred from a hole-trapped PO_4 tetrahedron. However, their peak wavelengths were very close together (Yokota and Imagawa, 1967). It was not easy to distinguish the wavelength peak of the Ag^{++} center from that of the Ag^0 center in the RPL spectra. The RPL appeared orange based on the luminosity function and had a peak value of unity at 555 nm. For the non-irradiated glass, intrinsic photoluminescence was scarcely connected to the radiation dose.

Fig. 4 shows the relation between the absorbed dose and the RPL intensity for the RPL glass particles. Five samples exposed to the same dose of gamma rays were prepared, and each RPL intensity value was measured. The representative value was normalized to the average of the five measurement values. The coefficient of variation was defined as the standard deviation divided by the average. It was confirmed that the RPL response had satisfactory linearity for doses up to 100 Gy. The radiation-induced optical absorption only weakly interfered with the RPL, although the transparency in the range from 500 to 900 nm was maintained at high doses. At a dose higher than 100 Gy, a correction of the light absorption coefficient was necessary for the confirmation of dose linearity. Meanwhile, the lowest detectable dose was 100 mGy, although this depended on the performance of the RPL readout system. For a commercial RPL readout system, the lowest detectable dose is effectively improved by a lifetime discrimination technique that reduces the pre-dose based on intrinsic photoluminescence (Maki et al., 2011). The intrinsic photoluminescence mainly decays with short-term components of <2 μs and long-term components of >20 μs (Piesch et al., 1986).

Fig. 5 shows changes of the RPL intensities at different temperatures measured by the photoluminescence measurement system. The temperature of each sample was kept constant within ±1 K. The X-ray generator was operated for 300 s, and the maximum absorbed dose was approximately 5 Gy. At 363 K, the increase in the RPL was recognized soon after the X-ray irradiation began. The RPL intensity was almost proportional to the absorbed dose. The RPL intensity was roughly constant after the X-ray irradiation. The RPL centers were promptly formed by the creation of electrons and holes. As for the samples at low temperatures, the increments of the RPL intensities evidently depended on the sample temperatures. The increment of the RPL intensity at 293 K was 15% of that at 363 K when the X-ray generator stopped. Then, the RPL intensity slightly increased after the X-ray irradiation. The results suggested that the formation of RPL centers had a temperature dependency.

3.2. Formation model of radiophotoluminescence centers

Indeed, the RPL intensity gradually increased with elapsed time after the RPL glass was irradiated at room temperature. This phenomenon is the so-called the “RPL buildup effect”. In silver-activated phosphate glass, the silver atoms exist uniformly and stably in the form of Ag^+ ions. Electrons and holes caused by ionizing radiation diffuse in the phosphate glass. Ag^0 and Ag^{++} centers are then formed as RPL centers. The Ag^0 center is easily formed at room temperature. The reaction speed for the formation of an Ag^{++} center is slower than that for Ag^0. The phosphate glass is formed by anions made of PO_4 tetrahedra and linked metal cations. The Ag^{++} center is transferred from a hole-trapped PO_4 tetrahedron. The hole mobility is low at room temperature. The RPL buildup effect is mainly constrained by the formation of Ag^{++} centers. The formation of Ag^{++} centers can be accelerated by a preheating process at approximately 343 K.

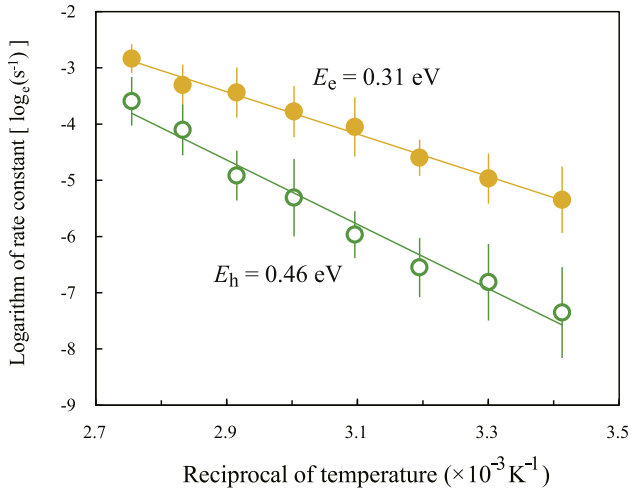

Fig. 6. Relation between the rate constant and the temperature. Each of the rate constants were determined by a curve fitting of the change in RPL intensity shown in Fig. 5. The higher activation energy of the rate constant, E_h, is 0.46 eV and corresponds to the formation of Ag^{++} center owing to the low hole mobility. The lower activation energy for the formation of Ag^0 center, E_e, is 0.31 eV.

Here, we have proposed an Arrhenius model, evolved from a previous model (Barthe and Blanc, 1979), for the formation of RPL centers. The RPL centers are assigned to Ag^+ ions trapping electrons or holes. The electrons and holes caused by ionizing radiation diffuse in the phosphate glass and induce the formation of Ag^0 and Ag^{++} as the RPL centers (Knežević et al., 2013):

$$Ag^+ + h^+PO_4 \rightarrow Ag^{++}, \quad (2)$$

$$Ag^+ + e^- \rightarrow Ag^0. \quad (3)$$

The reaction speed for the formation of Ag^{++} centers at room temperature is slow because the hole mobility is low. It is assumed that a precursor comprising an Ag^+ and a hole is produced at a stage prior to the formation of Ag^{++} centers. Under irradiation, the

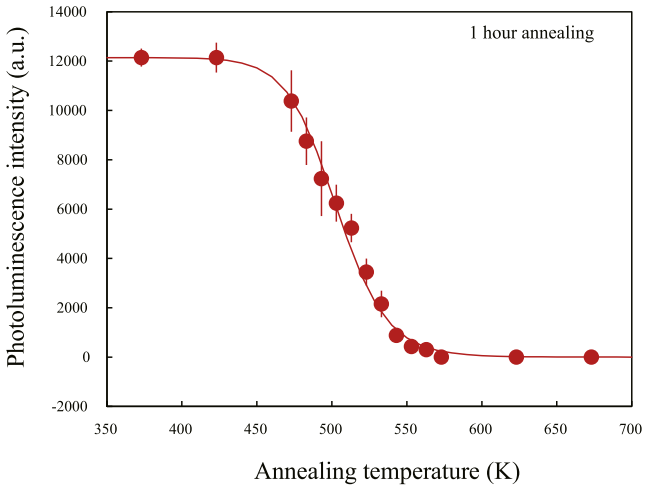

Fig. 7. Changes in RPL intensities after the annealing processes. Each of the annealing processes were carried out at a constant temperature for an hour. The RPL intensities were measured before and after the annealing process.

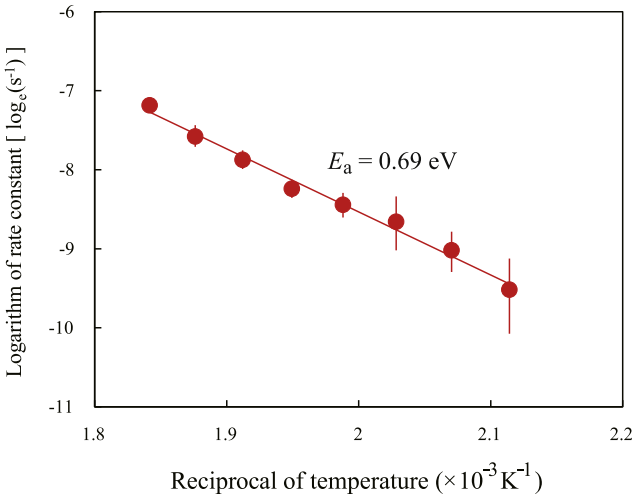

Fig. 8. Relation between rate constant for the extinction of RPL center and annealing temperature. The activation energy of the extinction of the RPL centers, E_a, is approximately 0.69 eV. In this model, E_a includes both of the RPL center types.

production rate of precursors is simply proportional to the dose rate φ and the number of Ag^{+} centers $[Ag^{+}]$. Ag^{++} centers are transformed from the precursors by a rate constant τ_h. The rate equation for the number of precursors, $[P_h]$, is given by

$$\frac{d[P_h]}{dt} = \sigma_h \varnothing \left[Ag^{+}\right] - \tau_h [P_h], \tag{4}$$

where σ_h is the cross section for the precursor per the dose. The rate equation for the number of Ag^{++} centers, $[Ag^{++}]$, is given by

$$\frac{d\left[Ag^{++}\right]}{dt} = \tau_h [P_h]. \tag{5}$$

If $[P_h]$ and $[Ag^{++}]$ are zero at $t = 0$, the number of Ag^{++} centers, $[Ag^{++}]$, is expressed as

$$\left[Ag^{++}\right] = \sigma_h \varnothing \left(t - \frac{1 - e^{-\tau_h t}}{\tau_h}\right)\left[Ag^{+}\right]. \tag{6}$$

In a similar way, a precursor comprising an Ag^{+} and an electron is produced prior to the formation of the Ag^{0} center. The number of Ag^{0} centers, $[Ag^{0}]$, is also determined by rate equations for the formation of Ag^{0} centers. The number of RPL centers is then the sum of $[Ag^{++}]$ and $[Ag^{0}]$:

$$\left[Ag^{++}\right] + \left[Ag^{0}\right] = \varnothing \left[\sigma_h \left(t - \frac{1 - e^{-\tau_h t}}{\tau_h}\right) + \sigma_e \left(t - \frac{1 - e^{-\tau_e t}}{\tau_e}\right)\right]\left[Ag^{+}\right], \tag{7}$$

where σ_e is the cross section for a precursor comprising an Ag^{+} ion and an electron, and τ_e is the rate constant for Ag^{0} center formation ($\tau_h < \tau_e$). According to the Arrhenius law, each of the rate constants is given as a function of the temperature T and its activation energy as follows:

$$\tau_h = A_h e^{-\frac{E_h}{kT}}, \tag{8}$$

$$\tau_e = A_e e^{-\frac{E_e}{kT}}, \tag{9}$$

where A_h and A_e are the pre-exponential factors, E_h and E_e are the activation energies, and k is the Boltzmann constant.

The change in the RPL intensity, as shown in Fig. 5, can be expressed by Eq. (7). The rate constants were determined by curve fitting the changes of the RPL intensities. Fig. 6 shows the relation between the rate constant and the temperature. The changes in the RPL intensities were measured five times at the same temperature. The rate constant and the coefficient of variation were the average of five values and the standard deviation divided by the average, respectively. The plot of the natural logarithm of τ_h versus T^{-1} produced a straight line that was used to determine E_h. From Fig. 6, the activation energies are 0.31 and 0.46 eV. The higher activation energy corresponds to the formation of Ag^{++} centers owing to the low hole mobility. The activation energy is important in estimating the RPL buildup effect dependency on temperature. At ambient temperature, the RPL buildup effect exists for hours after irradiation (Dmitryuk et al., 1996). When a substantial number of RPL detectors is used to simultaneously monitor a high radiation field in the F1, the preheating process would be practically impossible. Even so, radiation dose values can be corrected with this formation model. The rate constant τ_h, which has units of s^{-1} and varies as a function of temperature, is important in the dose estimation without a preheating process. If the radiation exposure time for the RPL detectors is several times longer than the reciprocal of τ_h, the formation of RPL centers is almost completed. Therefore, the RPL intensity is simply proportional to the radiation dose. For shorter durations, a correction factor should be derived from Eq. (7) for the radiation dose estimation.

Fig. 7 shows changes in the RPL intensities after annealing processes. Each of the annealing processes was carried out at a constant temperature for an hour to remove RPL centers. The RPL intensities were measured before and after the annealing process. The RPL intensities obviously decreased at temperatures above

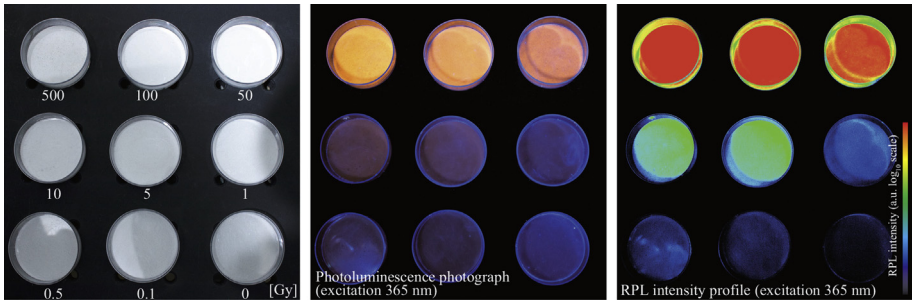

Fig. 9. Photographs of RPL glass particles exposed to ^{60}Co gamma rays. The RPL glass particles were set in petri dishes and covered with polystyrene plates. At doses above 5 Gy, orange photoluminescence could be recognized using the naked eye. In addition, the RPL was observed using a digital camera at doses above 0.5 Gy.

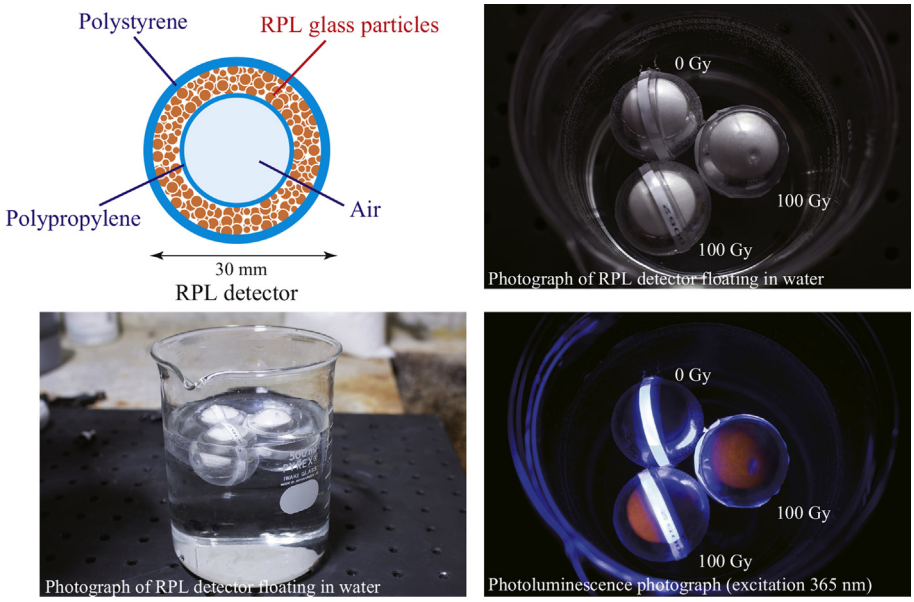

Fig. 10. Photographs of RPL glass particles encapsulated into polystyrene balls. Pulverized RPL glass particles were encapsulated into polystyrene balls 30 mm in diameter. Polypropylene floaters were centrically set inside the polystyrene balls, and the thickness of the layer of the RPL glass particles was 1–2 mm.

473 K. Fig. 8 shows the relation between the rate constant for the extinction of RPL centers and the annealing temperature. It is assumed that the number of RPL centers exponentially decays with a rate constant τ_a. Based on the Arrhenius law, the rate constant is expressed as

$$\tau_a = A_a e^{-\frac{E_a}{kT}}, \tag{10}$$

where A_a is the pre-exponential factor, and E_a is the activation energy of the extinction of the RPL centers. The activation energy is determined from the rate constant plot to be 0.69 eV and includes both of the RPL center types. The activation energy is slightly lower than the activation energy of the migration of silver atoms in phosphate glass, 0.72 eV (Maki et al., 2010).

3.3. *Visualization of high radiation field*

Fig. 9 shows photographs of RPL glass particles exposed to ^{60}Co gamma rays. The RPL glass particles were set in petri dishes 35 mm in diameter and covered with polystyrene plates 0.8 mm in thickness. At doses above 5 Gy, orange photoluminescence could be observed with the naked eye. In addition, the RPL was observed with the digital camera at doses above 0.5 Gy.

Fig. 10 shows photographs of polystyrene balls into which RPL glass particles were encapsulated. The RPL detectors floated in water due to their inner polypropylene floats. Orange luminescence from the RPL detectors was clearly observed under UV illumination. The RPL intensities were roughly corrected using the fluorescence intensities from the fluorescent marker tape on the polystyrene balls.

RPL photography was carried out after the ^{60}Co gamma-ray irradiation (Fig. 11). Fig. 12(a) shows a top-down photograph of 399 RPL detectors placed near the intense gamma-ray source. There were some lead blocks for radiation shielding. Fig. 12(b) shows the spatial radiation dose distribution calculated by a photon electron transport code, PHITS (Sato et al., 2013). Fig. 12(c) shows an RPL photograph of the RPL detectors 24 h after irradiation. The RPL detectors were uniformly brightened with the UV light illuminator, and a clear RPL photograph was taken by the digital camera. The

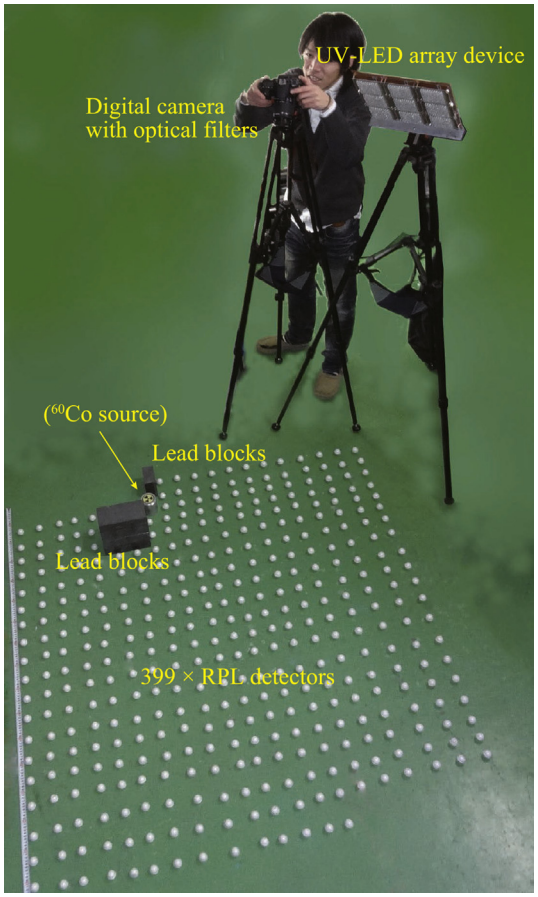

Fig. 11. RPL photography. Hundreds of RPL detectors were placed at 80 mm intervals around a 6 TBq ^{60}Co gamma-ray source in a 160 × 152 cm area. After irradiation, the RPL detectors were uniformly illuminated by a floodlight consisting of UV-LEDs, and photoluminescence images were recorded using a digital camera.

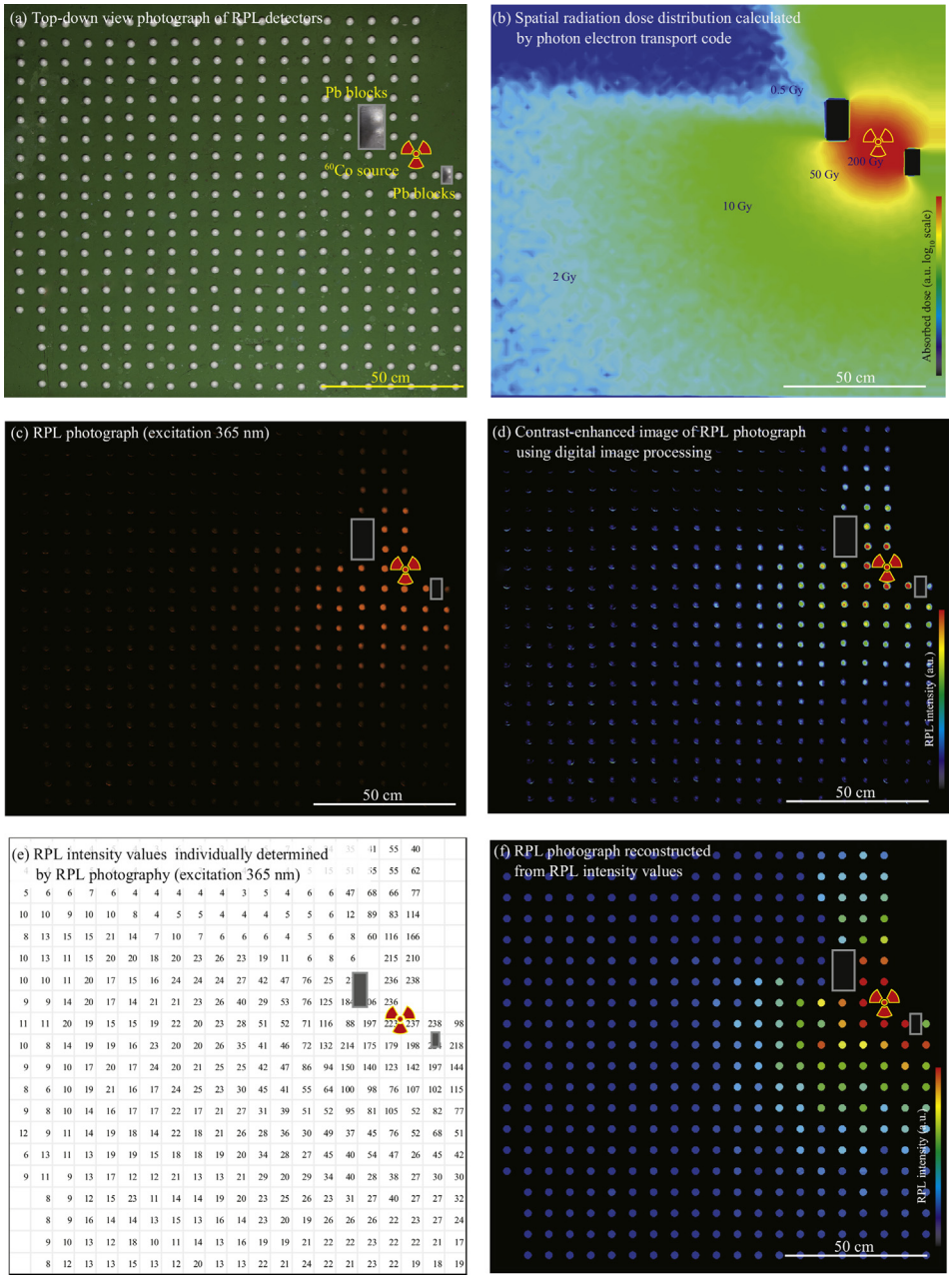

Fig. 12. Visualization of high radiation field by RPL photography. (a) A top-down view photograph of 399 RPL detectors placed near the intense gamma-ray source. There were some lead blocks placed for radiation shielding. (b) A spatial radiation dose distribution calculated by a photon electron transport code. (c) An RPL photograph of the RPL detectors 24 h following irradiation. The RPL detectors were uniformly illuminated by the UV-LED array device, and a clear RPL photograph was taken by the digital camera. At doses above 5 Gy, orange photoluminescence was clearly observed near the gamma-ray source with our naked eyes. (d) A contrast-enhanced image of the RPL photograph using digital image processing. (e) RPL intensity values individually determined by RPL photography. (f) An RPL photograph reconstructed from the RPL intensity values.

image contrast of the RPL photograph was improved due to the non-intrinsic blue photoluminescence that was effectively eliminated with color filters. At doses above 5 Gy, orange photoluminescence was clearly observed near the gamma-ray source with our naked eyes. Fig. 12(d) shows a contrast-enhanced image of the RPL photograph after digital image processing. The gradation of the radiation dose was obviously confirmed around the gamma-ray source. Fig. 12(e) shows RPL intensity values of the RPL detectors. Each of the RPL intensity values was individually determined using RPL photography. Fig. 12(f) shows an RPL photograph reconstructed from the RPL intensity values. The result was roughly consistent with those from the RPL photography, as shown in Fig. 12(c). Thus, the RPL photographing technique is expected to be useful for the visualization of high radiation fields.

4. Conclusion

Silver-activated phosphate glass was made from reagent-grade powders of $NaPO_3$, $Al(PO_3)_3$ and AgCl using a melting method. Its practical RPL property was investigated for the establishment of an RPL photographing technique. RPL glass samples were exposed to ^{60}Co gamma rays. Optical absorption bands at 315 and 360 nm were observed at high radiation doses. Meanwhile, there was little optical absorption in the wavelength

range from 500 to 900 nm. The radiation-induced optical absorption hardly interfered with the RPL, which exhibited a large peak at approximately 635 nm. Therefore, the RPL response had satisfactory linearity up to 100 Gy.

The RPL buildup effect was investigated using a photoluminescence measurement system with an X-ray generator. The increments of the RPL intensities evidently depended on the sample temperatures. At low temperatures, the RPL intensities slightly increased after irradiation. This temperature dependence was based on the formation mechanisms of the RPL centers (Ag^{++} and Ag^{0}). A formation model for the RPL centers was proposed to evaluate the RPL buildup effects. Two activation energies given in the formation model are 0.31 and 0.46 eV. The activation energies are essential to estimate the RPL buildup effects. In addition, the activation energy for the removal of RPL centers is approximately 0.69 eV. These parameters are important for the RPL photographing technique.

Pulverized RPL glass particles were encapsulated into hundreds of polystyrene balls of RPL detectors. The RPL detectors were placed near an intense ^{60}Co gamma-ray source. After irradiation, the RPL detectors were uniformly illuminated using a UV-LED array device. A clear RPL photograph was taken with a digital camera. At doses above 5 Gy, orange RPL could be recognized with the naked eye.

This simple RPL photographing technique is expected to be useful for the visualization of high radiation fields in the F1.

Acknowledgments

The authors are extremely grateful to our colleagues, Tadaaki Nagai, Souichi Tanaka and Satoshi Hisakado, for their contribution to the characterization of the RPL glass materials. This study was supported in part by System Development Program for Advanced Measurement and Analysis, Japan Science and Technology Agency (JST).

References

Aoi, Y., Kuchimaru, T., Maki, D., Sato, F., Ikeda, T., Kato, Y., Yamamoto, T., Iida, T., 2009. Radiophotoluminescent observation of X-ray microbeam track in silver-activated phosphate glass. Jpn. J. Appl. Phys. 48, 056001.

Barthe, J., Blanc, D., 1979. Model for the establishment of radiophotoluminescence in silver activated meta phosphate glasses. J. Lumin. 18/19, 396–401.

Dmitryuk, A.V., Paramzina, S.E., Perminov, A.S., Solov'eva, N.D., Timofeev, N.T., 1996. The influence of glass composition on the properties of silver-doped radiophotoluminescent phosphate glasses. J. Non-Cryst. Solids 202, 173–177.

Knežević, Ž., Stolarczyk, L., Bessieres, I., Bordy, J.M., Miljanića, S., Olko, P., 2013. Photon dosimetry methods outside the target volume in radiation therapy: Optically stimulated luminescence (OSL), thermoluminescence (TL) and radiophotoluminescence (RPL) dosimetry. Radiat. Meas. 57, 9–18.

Kurobori, T., Nakamura, S., 2012. A novel disk-type X-ray area imaging detector using radiophotoluminescence in silver-activated phosphate glass. Radiat. Meas. 47, 1009–1013.

Lee, M.S., Liao, Y.J., Huang, Y.H., Lee, J.H., Hung, S.K., Chen, T.R., Hsu, S.M., 2011. Radiation characteristics of homemade radiophotoluminescent glass dosimeter. Radiat. Meas. 46, 1477–1479.

Maki, D., Kobayashi, H., Sato, F., Murata, I., Kato, Y., Yamamoto, T., Iida, T., 2010. New radiophotoluminescence glass dosimeter with specialized radiation-sensitive surface layer. Jpn. J. Appl. Phys. 49, 116401–1-5.

Maki, D., Sato, F., Kato, Y., Yamamoto, T., Iida, T., 2011. Improvement of a dose reading system for radiophotoluminescence glass dosimeters. Radioisotopes 60, 55–61.

Miyamoto, Y., Yamamoto, T., Kinoshita, K., Koyama, S., Takei, Y., Nanto, H., Shimotsuma, Y., Sakakura, M., Miura, K., Hirao, K., 2010. Emission mechanism of radiophotoluminescence in Ag-doped phosphate glass. Radiat. Meas. 45, 546–549.

Piesch, E., Burgkhardt, B., Fischer, M., Rober, H.G., Ugi, S., 1986. Properties of radiophotoluminescent glass dosimeter systems using pulsed laser UV excitation. Radiat. Prot. Dosim. 17, 293–297.

Ranogajec-Komor, M., Knezevic, Z., Miljanic, S., Vekic, B., 2008. Characterisation of radiophotoluminescent dosimeters for environmental monitoring. Radiat. Meas. 43, 392–396.

Sato, F., Kuchimaru, T., Ikeda, T., Shimizu, K., Kato, Y., Yamamoto, T., Iida, T., 2008. X-ray microbeam measurement with radiophotoluminescent glass plate for single cell irradiation. Radiat. Meas. 43, 912–916.

Sato, T., Niita, K., Matsuda, N., Hashimoto, S., Iwamoto, Y., Noda, S., Ogawa, T., Iwase, H., Nakashima, H., Fukahori, T., Okumura, K., Kai, T., Chiba, S., Furuta, T., Sihver, L., 2013. Particle and heavy ion transport code system PHITS, version 2.52. J. Nucl. Sci. Technol. 50 (9), 913–923.

Yokota, R., Imagawa, H., 1967. Radiophotoluminescence centers in silver-activated phosphate glass. J. Phys. Soc. Jpn. 23, 1038–1048.